Does absorption against AGN reveal supermassive black hole accretion?

Tom Rose [1,2]★ B. R. McNamara,[1,2] F. Combes,[3] A. C. Edge,[4] A. C. Fabian [5] M. Gaspari [6]
H. Russell,[7] P. Salomé,[3] G. Tremblay[8] and G. Ferland[9]

[1]*Department of Physics and Astronomy, University of Waterloo, Waterloo, ON N2L 3G1, Canada*
[2]*Waterloo Centre for Astrophysics, Waterloo, ON N2L 3G1, Canada*
[3]*LERMA, Observatoire de Paris, PSL Research Univ., College de France, CNRS, Sorbonne Univ., F-75 014 Paris, France*
[4]*Centre for Extragalactic Astronomy, Durham University, Durham DH1 3LE, UK*
[5]*Institute of Astronomy, Cambridge University, Madingly Road, Cambridge CB3 0HA, UK*
[6]*Department of Astrophysical Sciences, Princeton University, Princeton, NJ 08544, USA*
[7]*School of Physics & Astronomy, University of Nottingham, Nottingham NG7 2RD, UK*
[8]*Harvard-Smithsonian Center for Astrophysics, 60 Garden St, Cambridge, MA 02138, USA*
[9]*Department of Physics and Astronomy, University of Kentucky, Lexington, Kentucky 40506-0055, USA*

ABSTRACT

Galaxies often contain large reservoirs of molecular gas that shape their evolution. This can be through cooling of the gas – which leads to star formation, or accretion on to the central supermassive black hole – which fuels active galactic nucleus (AGN) activity and produces powerful feedback. Molecular gas has been detected in early-type galaxies on scales of just a few tens to hundreds of solar masses by searching for absorption against their compact radio cores. Using this technique, ALMA has found absorption in several brightest cluster galaxies, some of which show molecular gas moving towards their galaxy's core at hundreds of km s^{-1}. In this paper, we constrain the location of this absorbing gas by comparing each galaxy's molecular emission and absorption. In four galaxies, the absorption properties are consistent with chance alignments between the continuum and a fraction of the molecular clouds visible in emission. In four others, the properties of the absorption are inconsistent with this scenario. In these systems, the absorption is likely produced by a separate population of molecular clouds in close proximity to the galaxy core and with high inward velocities and velocity dispersions. We thus deduce the existence of two types of absorber, caused by chance alignments between the radio core and: (i) a fraction of the molecular clouds visible in emission, and (ii) molecular clouds close to the AGN, in the process of accretion. We also present the first ALMA observations of molecular emission in S555, Abell 2390, RXC J1350.3+0940, and RXC J1603.6+1553 – with the latter three having $M_{mol} > 10^{10} M_{\odot}$.

Key words: ISM: molecules – galaxies: ISM – quasars: absorption lines.

1 INTRODUCTION

Most early-type galaxies at the centres of clusters lie within a hot, X-ray emitting atmosphere. The molecular gas that condenses as this atmosphere cools may contribute to star formation, or migrate towards the centre of the galaxy where it can fuel active galactic nucleus (AGN) activity. As a result of this fuelling, the AGN produces powerful radio jets and lobes which propagate energy into the galaxy cluster. This can then prevent further gas cooling and stifle the formation of molecular gas (McNamara et al. 2016; Morganti 2017; Gaspari, Tombesi & Cappi 2020). In massive galaxies, the molecular gas therefore acts as a medium through which many different processes are linked, so it is integral to our understanding of the galaxies and clusters.

The properties of this cooled gas have been predicted from a theoretical perspective (e.g. Nulsen et al. 2005; Pizzolato & Soker

2005; McNamara et al. 2016), studied with simulations (e.g. Gaspari, Ruszkowski & Oh 2013), and directly observed with emission lines (e.g. Crawford et al. 1999; Edge et al. 2002; Jaffe, Bremer & Baker 2005; Donahue et al. 2011; Olivares et al. 2019). These wide-ranging studies cover regions as large as clusters, and as small as individual clouds.

Theories and simulations typically cover a wide range of spatial scales, but observational studies tend to be more limited because molecular emission lines are relatively weak. This means they can only detect gas in large quantities. Outside our own galaxy, they therefore struggle to reveal how it behaves in compact regions. To some degree, this issue has been tackled with studies of molecular absorption lines. These are the shadows of gas clouds which lie in front of a bright and compact background radio source, such as a quasar. Observing molecular gas with this technique was pioneered with studies of the chance alignment of a foreground galaxy and the distant radio loud quasar PKS1830−211 (Wiklind & Combes 1996). Several similar absorption line systems have been found, but due to the necessity of a chance alignment between a galaxy and a

★ E-mail: thomas.rose@uwaterloo.ca

Table 1. The ALMA observations presented in this paper.

Source	RA (J2000)	Dec. (J2000)	Ang. res. (')	FOV (')	Int. time (s)	Obs. date (yyyy-mm-dd)	PWV (mm)	Line	Project code
NGC6868	20:09:54.1	−48:22:46.3	0.111	25	1421	2021-11-20	1.32	CO(2–1)	2021.1.00766.S
S555	05:57:12.5	−37:28:36.5	0.87	56	2812	2018-01-23	2.27	CO(1–0)	2017.1.00629.S
Hydra-A	09:18:05.7	−12:05:44.0	2.07	57	2661	2018-07-18	2.78	CO(1–0)	2017.1.00629.S
Hydra-A	09:18:05.6	−12:05:44.0	0.262	26	5745	2018-10-30	0.96	CO(2–1)	2018.1.01471.S
A2390	21:53:36.8	+17:41:43.7	0.52	59	8014	2018-01-07	2.08	CO(1–0)	2017.1.00629.S
A1644	12:57:11.6	−17:24:34.1	2.26	57	2752	2018-08-21	1.43	CO(1–0)	2017.1.00629.S
IC 4296	13:36:39.1	−33:57:57.3	0.40	25	1724	2014-07-23	1.64	CO(2–1)	2013.1.00229.S
Abell 2597	23:25:19.7	−12:07:27.7	0.43	26	10 886	2013-11-17	1.59	CO(2–1)	2012.1.00988.S
NGC5044	13:15:24.0	−16:23:07.6	0.74	54	2388	2018-09-20	0.49	CO(1–0)	2017.1.00629.S
NGC5044	13:15:24.0	−16:23:07.6	1.89	25	1421	2012-01-13	1.44	CO(2–1)	2011.0.00735.S
RXC J1350.3+0940	13:50:22.1	+09:40:10.7	0.89	61	5625	2018-09-16	0.66	CO(1–0)	2017.1.00629.S
MACS 1931.8−2634	19:31:49.6	−26:34:33.0	0.34	63	5322	2018-01-02	3.12	CO(1–0)	2017.1.00629.S
RXC J1603.6+1553	16:03:38.1	+15:54:02.4	0.83	60	1452	2018-09-16	0.82	CO(1–0)	2017.1.00629.S

bright background continuum source, the number of these detections remains small (other examples include Muller & Guelin 2008; Muller et al. 2013).

More recently, several systems have been found that use a galaxy's own radio core as a backlight, something for which only ALMA has been able to provide the necessary angular resolution and sensitivity (David et al. 2014; Tremblay et al. 2016; Rose et al. 2019a, b, 2020). In these studies, the compactness of the background radio source is particularly important because it makes it possible to detect gas on small scales. For example, in the brightest cluster galaxy Hydra-A, individual clouds of just a few tens of solar masses and with velocity dispersions of $\sim$1–5 km s^{-1} (Rose et al. 2020) have been found. In this respect, and in terms of their column densities, the individual clouds detected in this massive galaxy have remarkably similar properties to those seen in the Milky Way. This is surprising considering the extreme differences between the two galaxies in terms of their mass, star formation rates, AGN activity, and jet powers.

Absorption lines detected using a galaxy's own radio core as a backlight are particularly advantageous because the redshift of the line can be used to infer inward or outward movement of the gas. Rose et al. (2019b) found that from the nine known absorption line systems of this type, with a total of 15 individually resolved absorption regions detected, the gas tends to be in motion towards the galaxy core. Additionally, it has been suggested that the absorbing gas is likely in the innermost few hundred parsecs of the galaxies (Rose et al. 2019b). In cases where the gas has inward velocities of hundreds of km s^{-1}, the suggested proximity to the galaxy cores has been used to infer ongoing supermassive black hole accretion (e.g. Tremblay et al. 2016; Rose et al. 2019b).

In this paper, we constrain the likely location of the gas detected via molecular absorption lines in eight brightest cluster galaxies. Seven of these systems were part of the Rose et al. (2019b) ALMA survey which aimed to detect CO(1–0) absorption against each galaxy's central continuum source. This survey's targets were chosen because they had the strongest X-ray emission among the brightest cluster galaxies visible to ALMA. This meant bright continuum sources could be observed without orientation effects biasing the potential detections of absorption lines. In two of those sources, NGC 5044 and Abell 2597, no CO(1–0) absorption was detected. However, CO(2–1) absorption against their radio cores had previously been found (David et al. 2014; Tremblay et al. 2016). The eighth galaxy presented in this paper, IC 4296, was identified as an absorber when its CO(2–1) emission was observed by ALMA (Boizelle et al. 2017).

We constrain the location of the detected gas by analysing galaxies in which both molecular absorption and emission features have been detected. In the majority of cases, the absorption lines we analyse have previously been published, and some have also had their molecular emission lines studied in detail. However, we now use the data to investigate links between the molecular gas visible in absorption and the molecular gas visible in emission. We also present CO emission data for three galaxies that were part of the Rose et al. (2019b) survey hunting for molecular absorption lines, but in which only emission was found. These galaxies have molecular masses of $>10^{10}$ M$_\odot$, but lack absorption lines.

Throughout this paper, we assume Λ cold dark matter cosmology with $\Omega_M = 0.3$ and $\Omega_\Lambda = 0.7$, and a Hubble constant of $H_0 = 70$ km s^{-1} Mpc^{-1}.

2 OBSERVATIONS AND DATA REDUCTION

We present ALMA observations of molecular gas in 11 brightest cluster galaxies at redshifts in the range $z = 0.009$–0.35. Details of these observations are shown in Table 1. All but one have previously appeared in multiple publications, the most relevant of which are as follows. The molecular emission and absorption lines of NGC5044 have been studied in several papers, including David et al. (2014), Temi et al. (2018), and Schellenberger et al. (2020). Similar work focusing on Abell 2597 has also been carried out by Tremblay et al. (2018). The molecular absorption lines of S555, Abell 2390, Abell 1644, and NGC6868 have been presented in Rose et al. (2019b), but little attention was paid to their emission lines. This paper also presented the CO(1–0) emission lines of RXC J1350.3+0940, MACS 1931.8−2634, and RXC J1603.6+1553, but they were not studied in detail. Recently, Baek et al. (2022) carried out a multiwavelength study of Abell 1644, which includes the study of its molecular emission and absorption lines. Hydra-A has the largest number of molecular lines detected in any of our sources, with absorption from 11 different molecular species having been found by Rose et al. (2020). The molecular emission of Hydra-A has also been presented by Rose et al. (2019a). IC 4296 has absorption and emission lines that have been presented by Boizelle et al. (2017) and Ruffa et al. (2019).

All observations were handled using CASA version 6.4.0.16, a software package which is produced and maintained by the National Radio Astronomy Observatory (NRAO; McMullin et al. 2007). Self-calibrated measurement sets of the data were provided upon request to The European ALMA Regional Centre. From these, we produced

Table 2. Properties of the ALMA images presented in this paper, produced using the observations listed above.

Source	Continuum flux density (mJy)	Continuum frequency (GHz)	RMS noise (mJy/beam)	Channel width (km s^{-1})	Beam size (')
NGC6868	38	107	0.9	2.6	0.17×0.14
S555	31	103	0.5	2.6	0.64×0.53
Hydra-A	99	103	1.0	2.7	2.32×1.65
Hydra-A	70	218	0.9	0.7	0.27×0.20
A2390	21	98	0.3	3.1	0.71×0.57
A1644	63	103	0.7	2.6	2.27×1.54
IC 4296	191	234	0.5	1.3	0.63×0.57
Abell 2597	14.6	221	0.9	0.7	0.74×0.55
NGC5044	31	107	0.6	2.5	0.54×0.47
NGC5044	50	228	1.3	0.6	2.15×1.24
RXC J1350.3+0940	25	95	0.3	2.9	1.17×0.84
MACS 1931.8−2634	8.0	92	0.2	3.4	1.24×0.98
RXC J1603.6+1553	108	97	0.6	2.8	1.03×0.79

continuum subtracted images using the CASA tasks `tclean` and `uvcontsub`. In `tclean`, we have used a hogbom deconvolver, natural weighting and produced images with the smallest possible channel width. In Table 2, we show the key properties of our reduced images, including continuum flux densities estimated using channels free of emission and absorption.

When converting the frequencies of the CO spectra to velocities, we use rest frequencies of $f_{\text{CO(1-0)}} = 115.271208$ GHz and $f_{\text{CO(2-1)}} = 230.538000$ GHz.

3 MOLECULAR GAS PROPERTIES

In Figs 1 and 2, we show the galaxies in our sample that have CO emission and absorption lines. The left half of each panel contains two spectra. One is extracted from the region over which molecular gas is visible. In some cases where the absorption is strong enough to wipe out some of the more extended emission, this extraction region excludes the radio core (these cases are made clear in the legends). The second spectrum for each source is extracted from an approximately beam-sized region centred on the radio core. This extraction region maximizes the signal-to-noise ratio of the molecular absorption lines.

The right half of each panel shows two maps of the molecular gas. One is produced using the full velocity range over which emission is visible, and the second is produced using the velocity range in which molecular absorption is present, as indicated by the grey band in the left-hand panel. These maps are made using 'includepix = [0,100]' in CASA's `immoments` task. With these values the includepix parameter isolates flux between 0 Jy and an arbitrarily large value of 100 Jy. The cubes on which this task is performed are continuum subtracted, so any absorption takes on a negative value and is ignored by `immoments`. This prevents the absorption wiping out emission at velocities outside of the absorption region (for the sources in which the spectrum against the radio core contains both emission and absorption). Because this masks all negative values, it also has the effect of unevenly removing the noise. To account for this, the mean pixel value of the moments map is calculated in an off-centre, emission free region and then subtracted from the entire image. In some cases, the moments maps on the right show that there is no detectable molecular emission along the line of sight to the galaxy's radio core with velocities matched to the absorption lines.

In Fig. 3, we also show velocity and velocity dispersion maps of these galaxies made using $>3\sigma$ emission. These are made after

binning the spectral cubes to ≈ 10 km s^{-1} resolution and applying Gaussian smoothing over the beam area.

3.1 Molecular masses

The molecular mass of a galaxy with CO emission can be estimated using the following relation from Bolatto, Wolfire & Leroy (2013),

$$M_{\text{mol}} = \frac{1.05 \times 10^4}{F_{ul}} \left(\frac{X_{\text{CO}}}{2 \times 10^{20} \frac{\text{cm}^{-2}}{\text{K km s}^{-1}}} \right) \left(\frac{1}{1+z} \right)$$
$$\times \left(\frac{S_{\text{CO}} \Delta v}{\text{Jy km s}^{-1}} \right) \left(\frac{D_{\text{L}}}{\text{Mpc}} \right)^2 \text{M}_{\odot}, \quad (1)$$

where M_{mol} is the mass of molecular hydrogen, X_{CO} is the CO-to-H$_2$ conversion factor, z is the redshift of the source, $S_{\text{CO}} \Delta v$ is the CO emission integral, and D_{L} is the luminosity distance in Mpc. F_{ul} is a factor which is included as an approximate conversion between the expected flux density ratios of the CO(1–0) and CO(2–1) lines, where u and l represent the upper and lower levels. For CO(1–0), $F_{10} = 1$ and for CO(2–1), $F_{21} = 3.2$. This value is consistent with similar studies (e.g. David et al. 2014; Tremblay et al. 2016), and originates from a combination of the factor of 2 between the frequencies of the lines and the brightness temperature ratio observed for molecular clouds in spiral galaxies of 0.8 (Braine & Combes 1992).

The CO-to-H$_2$ conversion factor is a considerable source of uncertainty. To ensure our mass estimates are comparable with other similar studies, we use the standard Milky Way value of $X_{\text{CO}} = 2 \times 10^{20}$ cm^{-2} (K km s^{-1})$^{-1}$ in our calculations.

Table 3 shows the molecular gas masses of the eight galaxies shown in Figs 1 and 2. We also show the redshift and molecular gas velocity. Some of these sources have previously had their molecular gas masses estimated, but we repeat the calculations here for completeness. We also estimate the molecular masses of three brightest cluster galaxies which have emission lines but no absorption lines. These were first presented in Rose et al. (2019b), but no analysis of them was carried out. These three galaxies are discussed later in Section 3.2.

The stellar redshifts of Hydra-A, Abell 1644, and NGC 5044 are taken from Multi Unit Spectroscopic Explorer (MUSE) observations (ID: 094.A-0859). The MUSE stellar redshift we use for Abell 2597 is consistent with the value from Ca II, H+K absorption lines (Voit & Donahue 1997). The stellar redshifts of RXC J1350.3+0940 and RXC J1603.6+1553 are derived from a combination of emission and absorption lines detected with the
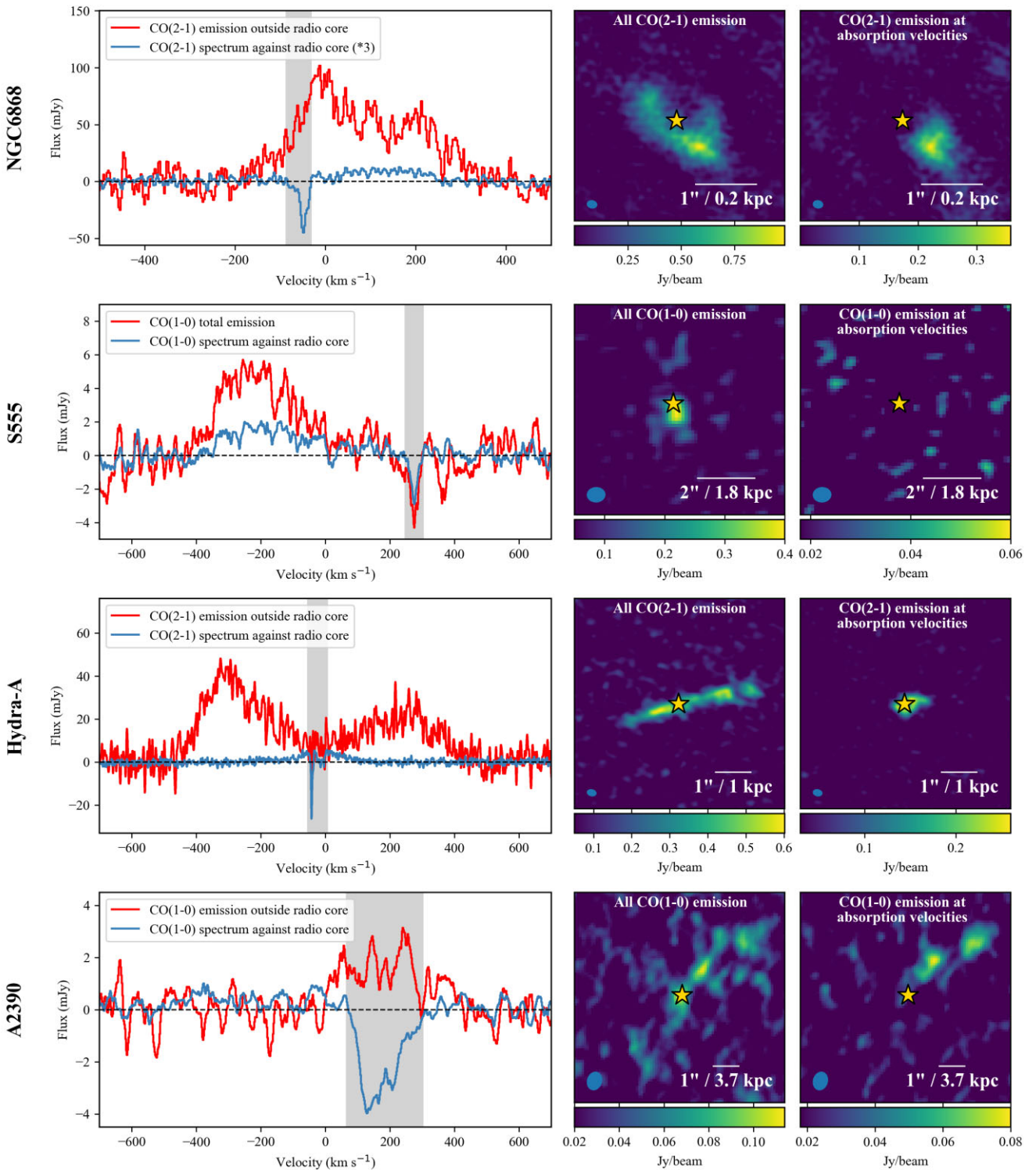
Figure 1. Galaxies with molecular absorption lines seen against their bright and compact radio core. *Left*: Red lines show CO spectra extracted from the region over which molecular gas is visible. This sometimes excludes the core region when the absorption is particularly strong (these cases are made clear in the legends). Blue spectra, which show the molecular absorption, are extracted from an approximately beam-sized region centred on each object's continuum source (the location of which is indicated by the yellow star). *Right*: CO intensity maps made using (i) the full range of velocity channels in which molecular emission is observed, and (ii) the velocity channels in which molecular absorption is observed, as indicated by the grey band.
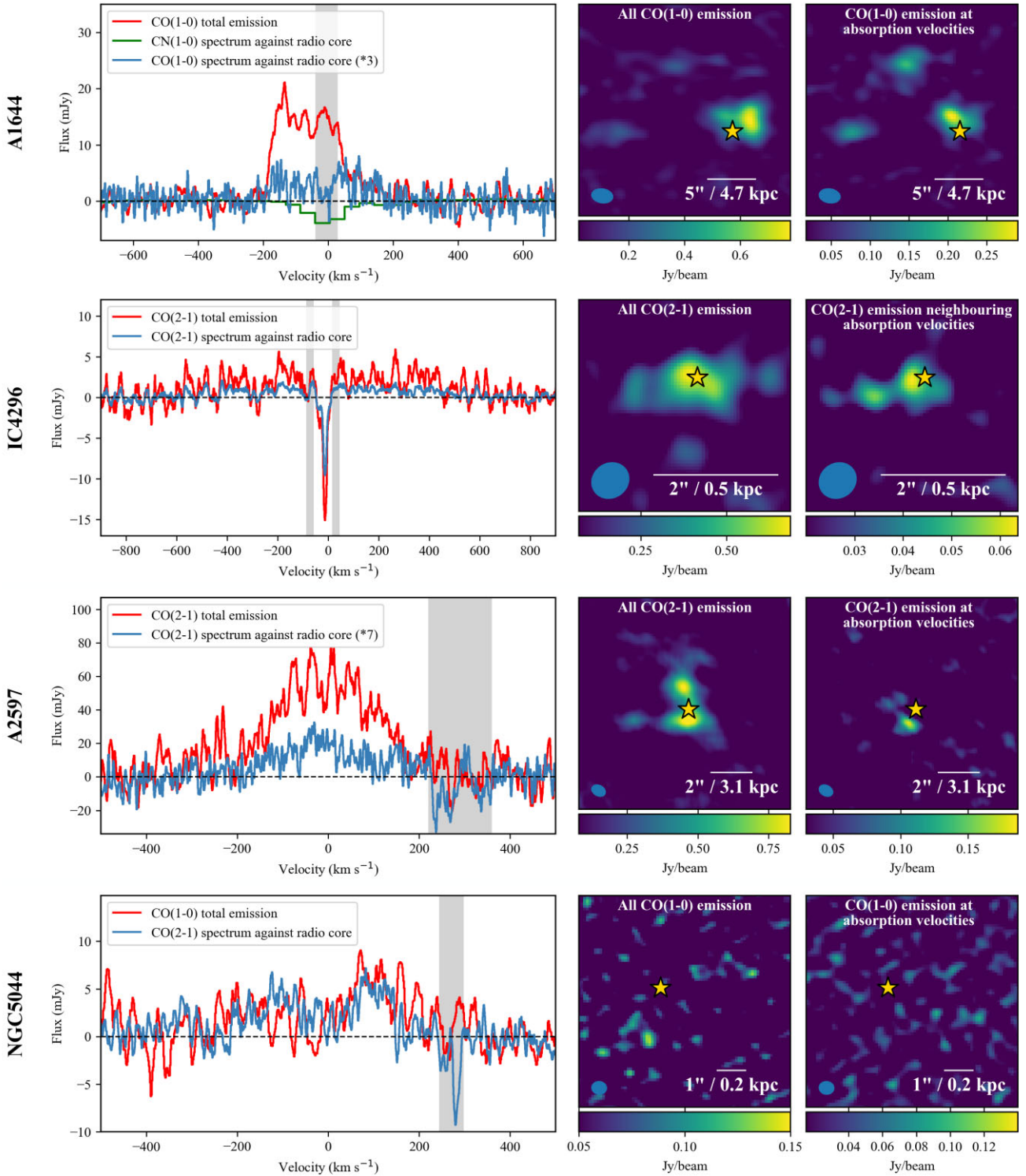
Figure 2. Continued from Fig. 1. Additional information: **A1644** has a complex CO(1–0) profile against its radio core that contains both emission and absorption. We therefore include the much stronger CN absorption line as a visual guide. However, this has much lower spectral resolution and contains hyperfine structure, which increases its apparent width. The intensity map on the right of **IC4296** is made with velocity channels neighbouring the absorption line. Using only the velocity channels in which absorption is seen is not possible because the emission is only marginally extended beyond the beam size. In **NGC5044**, the absorption and emission lines are most clearly visible in the CO(2–1) data. However, because this is of poor spatial resolution and we are particularly interested in the location of the gas, we made the intensity maps using the higher angular resolution CO(1–0) observation.
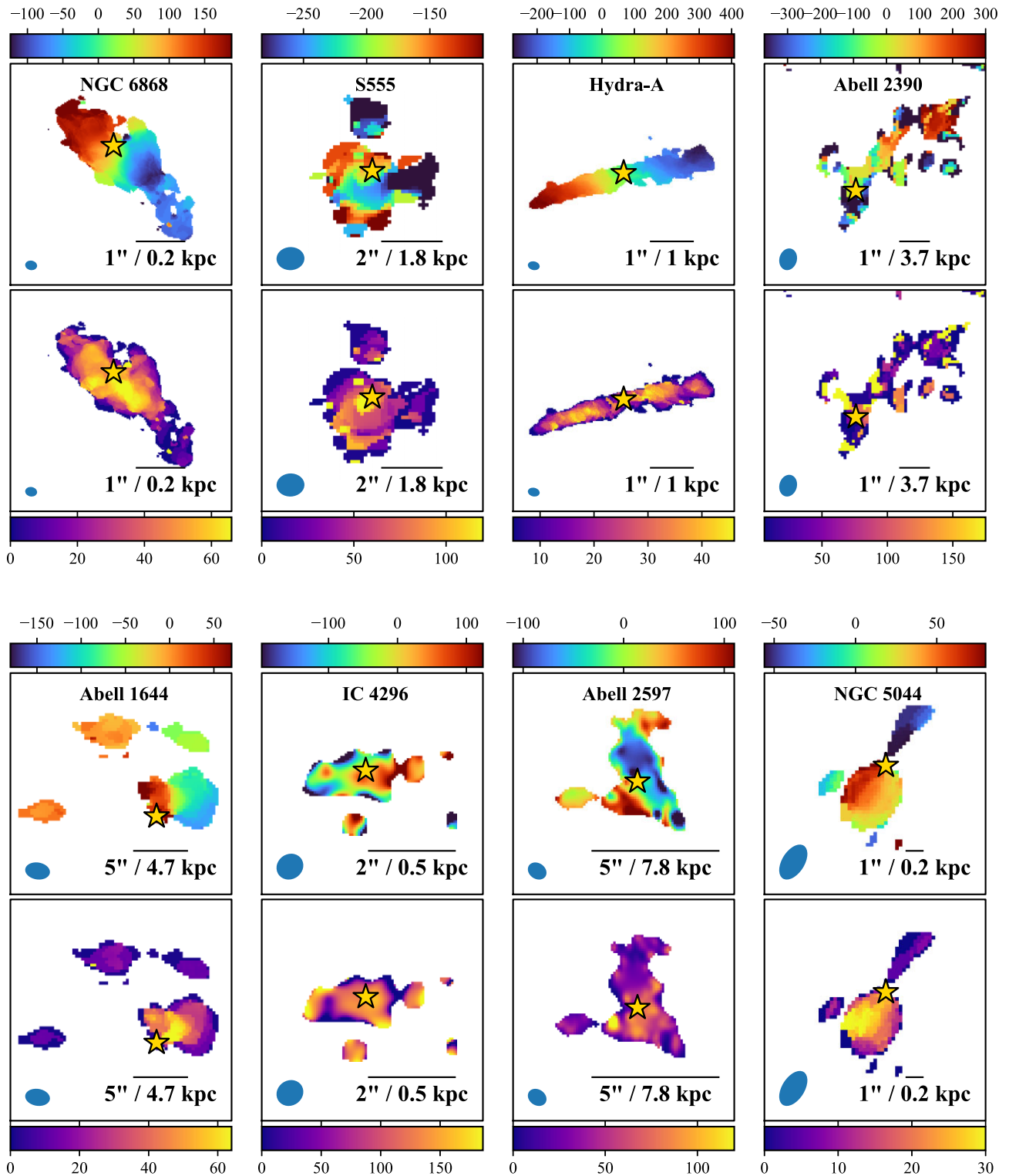
Figure 3. Velocity (upper) and dispersion (lower) maps for the eight galaxies in our sample with molecular absorption lines visible against their bright radio cores. Yellow stars indicate the position of each galaxy's radio core. All values in colour bars have units of $\mathrm{km\,s^{-1}}$. Note that while CO(1–0) data are shown for NGC 5044 in Fig. 2, we use the stronger CO(2–1) data to make velocity and velocity dispersion maps.

Table 3. Redshifts, their corresponding velocities, velocity offsets of the molecular gas, molecular emission line integrals and molecular masses. All redshifts are barycentric and use the optical convention.

Source	z_*	v_* (km s^{-1})	$v_* - v_{mol}$ (km s^{-1})	M_{mol} (M$_\odot$)
NGC 6868	0.0095 ± 0.0001 (FORS)	2830 ± 30	70 ± 40	$1.3 \pm 0.2 \times 10^8$
S555	0.0446 ± 0.0001 (MUSE)	$13\,364 \pm 30$	-190 ± 40	$5.6 \pm 0.5 \times 10^8$
Hydra-A	0.0544 ± 0.0001 (MUSE)	$16\,294 \pm 30$	120 ± 50	$3.1 \pm 0.2 \times 10^9$
Abell 2390	0.2304 ± 0.0001 (VIMOS)	$69\,074 \pm 30$	170 ± 40	$2.2 \pm 0.6 \times 10^{10}$
Abell 1644	0.0473 ± 0.0001 (MUSE)	$14\,191 \pm 30$	-60 ± 40	$1.6 \pm 0.3 \times 10^9$
IC 4296	0.01247 ± 0.00003 (NED)	3738 ± 10	-60 ± 50	$2.3 \pm 0.2 \times 10^7$
Abell 2597	0.0821 ± 0.0001 (MUSE)	$24\,613 \pm 30$	20 ± 40	$4.6 \pm 0.5 \times 10^9$
NGC 5044	0.0092 ± 0.0001 (MUSE)	2761 ± 30	30 ± 40	$2.4 \pm 0.4 \times 10^7$
RXC J1350.3+0940	0.13255 ± 0.00003 (SDSS)	$39\,737 \pm 10$	-60 ± 30	$2.5 \pm 0.3 \times 10^{10}$
MACS 1931.8−2634	0.35248 ± 0.00004 (MUSE)	$105\,670 \pm 10$	-20 ± 30	$7.8 \pm 0.7 \times 10^{10}$
RXC J1603.6+1553	0.10976 ± 0.00001 (SDSS)	$32\,905 \pm 3$	0 ± 30	$1.0 \pm 0.1 \times 10^{10}$

Sloan Digital Sky Survey (SDSS; Abazajian et al. 2009). The stellar redshift of MACS 1931.8−2634 is taken from Fogarty et al. (2019) and is found using MUSE observations. Cross-checking with FOcal Reducer and low dispersion Spectrograph (FORS) observations of S555, Abell 1644, NGC 5044, and Abell 2597 provides redshifts in good agreement with those listed. The redshifts used for Abell 2390 and RXCJ0439.0+0520 are taken from Visible Multi-Object Spectrograph (VIMOS) observations previously presented by Hamer et al. (2016) and are based primarily on stellar emission lines. The observed wavelengths of the single stellar absorption line in these two VIMOS spectra are consistent with the quoted redshifts. The redshifts we use here are the same as those given in Rose et al. (2019b). The exception to this is IC 4296, which was not presented in that paper. For this source, we have used the same value as Ruffa et al. (2019).

To estimate the molecular masses, we first make Gaussian fits to the emission lines extracted from the region over which molecular gas is visible. Depending on the profile of the emission, we use either a single Gaussian or double Gaussian line. For sources with absorption lines that are embedded within (or are near to) the emission, we mask the absorption before making the fits. The masked velocity range is the same as that shown by the grey band in Figs 1 and 2 (except in IC 4296, where we mask the range between the grey bands).

For most sources estimating the molecular mass is a straightforward process. However, A2390 and NGC 5044 require more detailed explanation.

A significant amount of emission in A2390 is in close proximity to the radio core. The observation also has a relatively large beam size and a wide molecular absorption line. If a spectrum is extracted from the entire region over which molecular emission is present, the absorption line wipes out the spatially extended molecular emission which is shown by the red line in Fig. 1. This results in a severely underestimated molecular mass. The molecular emission from the core region has a wider velocity range, and is still visible at velocities below that of the absorption (see the blue line in Fig. 1). We therefore extract spectra from two non-overlapping regions: one surrounding the radio core, and another which is more spatially extended. The masses from these two regions are then calculated following the procedure outlined above and summed together.

Molecular emission in NGC 5044 has been detected in both CO(1–0) and CO(2–1). The CO(2–1) line is the stronger of the two and has been analysed by David et al. (2014), Temi et al. (2018), and Schellenberger et al. (2020). Nevertheless, in Table 3 we present a new mass estimated from the spatially resolved CO(1–0) emission. We find a mass of $2.4 \pm 0.4 \times 10^7$ M$_\odot$ from a 6×2 arcsec

rectangular extraction region centred on the continuum and at an angle of 40 deg. This is similar to the value of $4.2 \pm 0.1 \times 10^7$ M$_\odot$ found by Schellenberger et al. (2020), from a circular radius of 6 arcsec. No CO(1–0) emission is clear from outside the rectangular extraction region used (see Fig. 2), but for completeness we also estimate the mass from within the 6 arcsec radius used by Schellenberger et al. (2020) on the CO(2–1) data. This gives a mass of $3.5 \pm 0.6 \times 10^7$ M$_\odot$, so some weak emission may in fact be present outside the rectangular region described. NGC 5044 also contains more spatially extended molecular gas visible to the ALMA Compact Array (ACA). From ACA observations, Schellenberger et al. (2020) find a mass of $6.5 \pm 0.2 \times 10^7$ M$_\odot$ within a 15 arcsec radius.

3.2 Three brightest cluster galaxies with $>10^{10}$ M$_\odot$ of molecular gas

The largest single survey searching for molecular absorption lines in brightest cluster galaxies was completed in ALMA Cycle 6 (project 2017.1.00629.S, PI Edge). In total, 20 sources were observed and eight had detections of molecular absorption against their radio cores (Rose et al. 2019b). Several of the targets from this survey in which molecular absorption was found are shown in Figs 1 and 2.

In three of the targets molecular emission was detected, but no absorption lines were found. We introduce them here and briefly discuss the properties of their molecular emission. Since these targets were observed as part of the same survey in which most of the absorbing sources were identified, they make for an interesting comparison.

In Fig. 4, we show their intensity, velocity, and velocity dispersion maps. Below we briefly summarize the properties of their molecular emission.

(i) **RXC J1350.3+0940** has $2.5 \pm 0.3 \times 10^{10}$ M$_\odot$ of molecular gas in a slightly inclined edge-on disc with a smooth velocity gradient, a velocity range of approximately 300 km s^{-1} and diameter of 10 kpc.

(ii) **MACS 1931.8−2634** has a molecular mass of $7.8 \pm 0.7 \times 10^{10}$ M$_\odot$ centred a few hundred parsecs from its radio core. There is no clear velocity structure. The gas has a roughly circular distribution with a diameter of approximately 5 kpc. The molecular gas of MACS 1931.8−2635 has previously been studied by Fogarty et al. (2019), though the CO(1–0) observation we present has not previously been published. With the Galactic X_{CO} conversion factor which we use throughout this paper, Fogarty et al. (2019) find a molecular mass of $9.4 \pm 1.3 \times 10^{10}$ M$_\odot$ from their CO(1–0) observation.
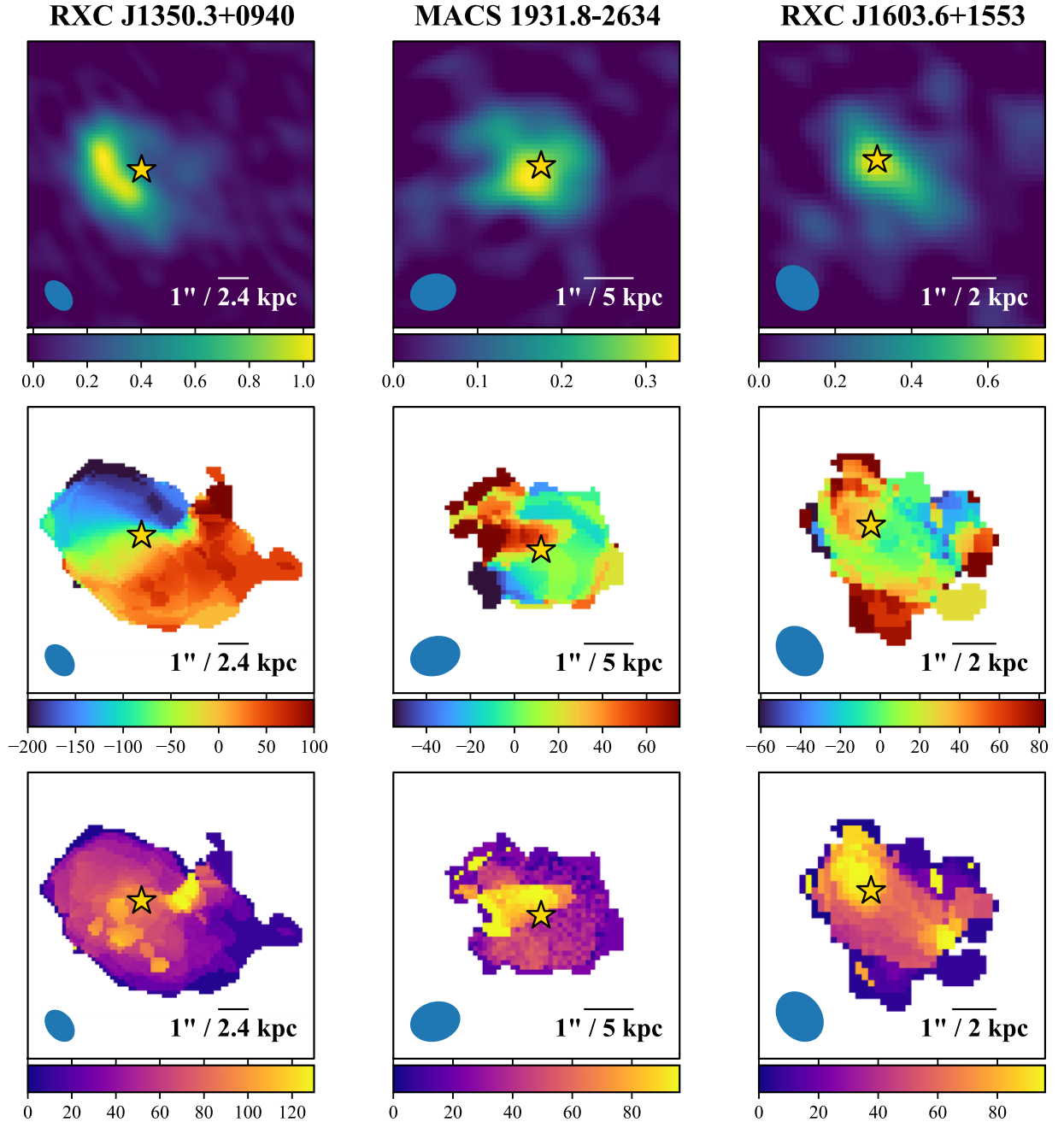
Figure 4. From top to bottom: Intensity, velocity, and velocity dispersion maps for three brightest cluster galaxies with $>10^{10}\,M_\odot$ of molecular gas, but no absorption. Units are Jy km s^{-1}, km s^{-1}, and km s^{-1}.

(iii) **RXC J1603.6+1553** has $1.0 \pm 0.1 \times 10^{10}\,M_\odot$ of molecular gas, with the brightest emission centred on its radio core. The gas is weakly resolved spatially but appears to extend across a diameter of around 5 kpc. There is no clear velocity structure.

The molecular masses in these systems are extremely high and make them among the most gas rich systems known (Pulido et al. 2018). All three also have strong emission coincident with their radio cores, so their lack of absorption features is surprising. This is particularly so given that galaxies with molecular masses lower by approximately two orders of magnitude (NGC 6868 and S555) have clear CO(1–0) absorption. NGC 5044 also has absorption, despite having no detectable emission along the line of sight to its radio core.

Therefore, the probability of seeing molecular absorption against a galaxy's radio core is not strictly dependent on the total amount of molecular gas present, but more so on the molecular column density and gas properties (such as the excitation temperature).

3.3 Column density estimates from emission

The blue spectra in Figs 1 and 2 are extracted from compact regions centred on each galaxy's continuum source. In all these spectra, emission is present. This suggests there may be a significant amount of molecular gas along the line of sight to the continuum.

However, the continuum sources are significantly smaller than the angular resolution of the observations. Therefore, although the

Table 4. The column density of molecular gas covering each galaxy's continuum source, estimated from emission and absorption seen along the line of sight. Due to uncertainties in constants used in calculations, all values carry an error of approximately 50 per cent. [1]The emission coincident with the continuum source in Abell 1644 is unresolved by an observation with a relatively large beam size, so we mark this column density as a lower limit.

	Column density		Clumping factor
	Emission	Absorption	
NGC 6868	960	1100	1.1
S555	130	1300	9.8
Hydra-A	530	210	0.4
Abell 2390	160	15 000	92
A1644[1]	>50	310	<6
IC 4296	170	290	1.1
Abell 2597	130	6800	54
NGC5044	<50	3800	>76
RXC J1350.3+0940	130	<700	<5.4
MACS 1931.8−2634	240	<2200	<9.5
RXC J1603.6+1553	330	<3400	<10

emission and absorption in these spectra are extracted from the same region, they originate on different spatial scales. Typically, the beam sizes are of arcsec scale, while continuum sources are of milliarcsec scale. As a result, any emission in these spectra will come from a physically much larger region than the absorption, so the two are not directly comparable.

The emission strength is also heavily dependent on factors such as redshift and beam size, so it is an unreliable indicator of how much gas is likely to be covering the continuum. However, these parameters are known accurately, so the average column density of emitting gas covering the continuum source can be found by assuming a uniform density within the beam. This then serves as an estimate of the column density of molecular gas covering the continuum source (unless there is a significant amount of molecular gas which is too cool to be visible in emission, as suggested by Fabian et al. 2022). The interstellar medium is clumpy, so this calculation will give an average column density across many different lines of sight. In reality, some lines of sight may intersect many clouds and have a higher column density. Other lines of sight may intersect with negligible amounts of gas.

When using a spectrum extracted from a beam sized region centred on the continuum source, the column density of molecular gas is

$$\sigma_{\rm mol} = \frac{M_{\rm mol}}{2A_{\rm beam}}\, {\rm M}_\odot\, {\rm pc}^{-2}, \qquad (2)$$

where $M_{\rm mol}$ is the mass in ${\rm M}_\odot$ estimated from equation (1), and $A_{\rm beam}$ is the beam area in pc^2. The factor of 2 accounts for only gas on one side of the galaxy being able to cover the continuum source, whereas the emission comes from gas on both sides.

In Table 4, we show the column density of molecular gas expected to cover each continuum source. Most of the estimated values are similar to the typical mass and column densities of giant molecular clouds. Lombardi, Alves & Lada (2010) find typical masses of 170 to 710 ${\rm M}_\odot$ for giant molecular clouds, while their column densities are found to be 50 ${\rm M}_\odot$ pc^{-2} in the Large Magellanic Cloud (Hughes et al. 2010) to 170 ${\rm M}_\odot$ pc^{-2} in the Milky Way (Solomon et al. 1987). In turn, this implies a low covering fraction of molecular clouds (as is also predicted by simulations, e.g. Gaspari, Temi & Brighenti 2017). Therefore, as previously stated, clumpiness may mean some lines of sight to the continuum intersect several molecular clouds, while others intersect none.

3.4 Column density estimates from absorption

The line-of-sight column density, $N_{\rm tot}$, of an optically thin molecular absorption region is

$$N_{\rm tot}^{\rm thin} = Q(T_{\rm ex})\frac{8\pi\nu_{ul}^3}{c^3}\frac{g_l}{g_u}\frac{1}{A_{ul}}\frac{1}{1 - e^{-h\nu_{ul}/kT_{\rm ex}}} \int \tau_{ul}\, dv\,, \qquad (3)$$

where $Q(T_{\rm ex})$ is the partition function, c is the speed of light, A_{ul} is the Einstein coefficient of the observed transition, and g is the level degeneracy, with the subscripts u and l representing the upper and lower levels (Godard et al. 2010; Mangum & Shirley 2015).

The assumption of optically thin absorption in equation (3) is inappropriate for some of our data. To account for this, a correction factor can be applied (Mangum & Shirley 2015) to give the following more accurate column density,

$$N_{\rm tot} = N_{\rm tot}^{\rm thin}\frac{\tau}{1 - \exp(-\tau)}. \qquad (4)$$

Equation (3) gives the column density of the absorbing molecule as a number density per square cm. To make these column densities comparable with those estimated from the emission in the previous subsection, we convert this to a column density in units of ${\rm M}_\odot$ pc^{-2}. This requires the assumption of an H$_2$/CO number ratio, which we assume to be constant across all of our sources. This ratio has been estimated using optically thin isotopologues, such as ^{13}CO. Observations of the Milky Way's Taurus molecular cloud by Pineda et al. (2010) give an estimate of CO/H$_2$ = 1.1 × 10^{-4} (with an assumed isotopic ratio of CO/^{13}CO = 70). Similarly, *Far Ultraviolet Spectroscopic Explorer* observations by Rachford et al. (2009) give a ratio of CO/H$_2$ = 1.8 × 10^{-4}. In our calculations, we use a ratio of CO/H$_2$ = 1.5 × 10^{-4}. We also assume an excitation temperature of 5 K. This is the approximate value for the absorbing clouds in Hydra-A (Rose et al. 2020).

Table 4 shows the column densities estimated using each object's molecular absorption lines. To calculate these we use the most optically thin line available in each case e.g. the weaker CO(1–0) line in Hydra-A from Rose et al. (2019a). We also show upper limits for the absorption column densities of the three sources from the Rose et al. (2019b) survey that have molecular emission but no detectable absorption. These upper limits are found assuming an absorption line with a velocity dispersion of $\sigma = 20$ km s^{-1}.

4 DISCUSSION

4.1 Two types of molecular absorption line system

In Section 3, we employed two methods to estimate the column density of molecular gas along the line of sight to each object's continuum source. First, we used the molecular emission, which indicates the amount of gas from the galaxy-scale distribution that is expected to cover the continuum. Secondly, we derived the column density from the absorption. This gives the actual amount of molecular gas that covers the continuum.

The clumping factors we find range from 0.4 (where just less than half as much absorbing gas is seen as would be expected on an average line of sight) to 92 (where 92 times as much gas is seen in absorption as would be expected on an average line of sight). We find no correlation between the clumping factor and the beam size or redshift. It is also worth noting that the clumping factors we find are heavily dependent on the excitation temperature and CO-to-H$_2$ conversion factor used. However, unless there is a large and unexpected variation in these values between individual sources, comparison of their relative values is meaningful.
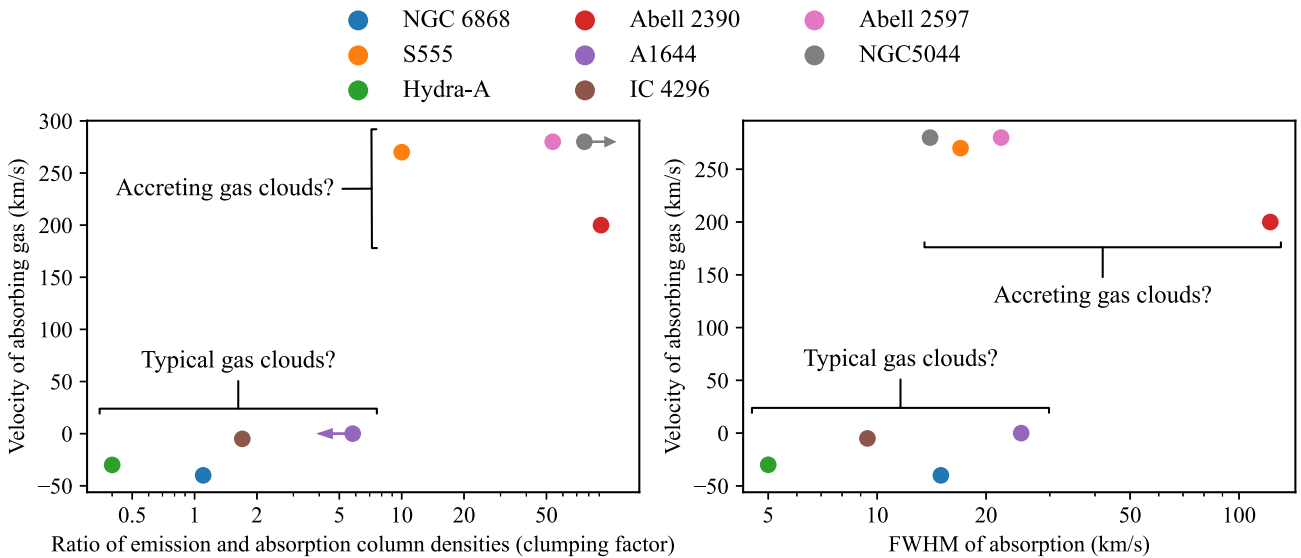
Figure 5. The clumping factor and FWHM of the absorbing gas versus its central velocity. Positive velocities mean inward motion towards the centre of the galaxy. The clumping factor is the ratio of two column density estimates derived from (i) the molecular emission from a beam-sized region spatially coincident with the radio core, and (ii) the molecular absorption against the radio core. A clumping factor of 1 implies that the absorption is tracing a column density equal to the average amount of emitting gas covering a line of sight to the continuum source. A clumping factor of 2 implies that twice as much gas is being traced. In the right-hand panel, for sources with multiple absorption features we use the FWHM of the deepest.

That having been said, if each source's absorption is caused by the same population of clouds as are responsible for the emission, the larger clumping factors imply that the absorption lines are tracing significantly more molecular gas than expected in these systems. Alternatively, the high variance may be explained by the clumpiness of the interstellar medium's molecular gas.

In Fig. 5, we show the clumping factor of each source (and the absorption's full width at half-maximum, FWHM) plotted against the mean absorption velocity. Two distinct populations are apparent. The first has clumping factors close to unity (narrow FWHM) and the absorbing gas is moving at close to 0 km s^{-1}. The velocity of the absorbing gas is also similar to that of the molecular emission. The second population has high clumping factors (wide FWHM) and the absorbing gas has high velocities towards the galaxy core. These velocities are dissimilar to that of the molecular emission (except in Abell 2390, where the emission is unusually wide at 900 km s^{-1}).

In the following sections, we argue that these two populations represent two distinct types of absorption system. The first contains absorption due to chance alignments between the continuum source and the galaxy-wide distribution of molecular gas – the same gas which is responsible for the galaxy's molecular emission. The second population contains absorption which is due to a distinct and much less numerous set of molecular clouds which are in the process of accreting on to the AGN. Due to the scarcity of these clouds, they are not visible in emission, but their proximity to the galaxy centre makes alignment with the continuum more likely.

4.2 The expected properties of molecular absorption lines

We have proposed that the absorption lines in Figs 1 and 2 are due to two distinct populations of molecular gas clouds – those spread throughout the galaxy and those at lower radii which are accreting on to the AGN. We now explain how the properties of the absorption caused by these two cloud populations arise.

4.2.1 Absorption due to clouds visible in emission (typical clouds)

A CO spectrum seen against the central continuum source of a galaxy can contain the following components (i) emission, produced by 10^7 M$_\odot$ or more of molecular gas lying across a region of several hundred parsecs, and (ii) absorption, produced by approximately several hundred to several thousand solar masses of molecular gas which lies along the narrow line of sight to the galaxy's bright radio core (e.g. Rose et al. 2020).

A significant column density is required for a fraction of the gas spread across a galaxy's disc to have a high probability of occulting the continuum and producing molecular absorption. Typically, molecular clouds in the Milky Way are clumpy and have column densities of around 170 M$_\odot$ pc^{-2} (Solomon et al. 1987). Therefore, for a continuum source a few square parsec in size, a column density of a few hundred M$_\odot$ pc^{-2} would be required for an alignment between the continuum and one or more molecular clouds to be probable – depending on the level of gas clumping. If there is an alignment, the velocity dispersion of a single cloud's absorption would likely be similar to that of molecular clouds in the disc of the Milky Way, i.e. rarely above 8 km s^{-1} (Miville-Deschênes, Murray & Lee 2017). It would also be similar to the velocity dispersion found for molecular clouds detected in galaxy discs when using a high redshift quasar as an absorption backlight, i.e. also rarely above 8 km s^{-1} (e.g. Wiklind & Combes 1996; Combes 2008; Muller et al. 2013). However, multiple closely associated molecular clouds with similar velocities may combine to produce a wider absorption feature.

Absorption due to chance alignments between the continuum source and a fraction of the clouds that are visible in emission will exist along an extremely narrow line of sight. However, the beam of any observation will be much larger than this and may contain enough molecular gas to be visible in emission. In these cases, the emission spectrum (i.e. velocity versus flux) can be interpreted as showing the relative number of clouds as a function of velocity. Clouds with a velocity at the peak of the emission are the most numerous, so clouds at these velocities would be the most likely to intersect the continuum.

Absorption at or close to the peak of the emission is therefore most likely in this situation. This will also be true for any absorption lines produced by extremely cool gas not visible in emission, assuming the cooler and warmer gas are dynamically linked.

Throughout the rest of this paper, we use the term 'typical' in reference to those clouds that make up a galaxy's molecular emission.

4.2.2 Absorption due to clouds close to the AGN

Absorption due to molecular clouds close to the centre of a galaxy are not forbidden from having similar characteristics to those expected of more typical clouds which are at larger radii, but in all likelihood their line-of-sight velocity and velocity dispersion will be different.

The relative probability of an absorption line being produced by a cloud in the core of a galaxy is considerably higher than it is for one further out. As simulations (such as Krumholz, Kruijssen & Crocker 2016; Gaspari et al. 2017) show, the volume filling factor and internal density of molecular clouds is inversely proportional to their distance from the galaxy centre. Since these clouds are more likely to occult the continuum than those at larger radii, they won't necessarily be sufficiently numerous to make them visible in emission. Therefore, the absorbing clouds need not have a similar velocity to the clouds visible in emission. Instead, due to their presence in the strong gravitational field, they can attain high inward velocities and be redshifted compared with the galaxy's emission.

A second way in which absorption from gas near the galaxy centre may differ is in its width. The nuclear region of a galaxy is a hostile environment with a large velocity gradient. This would quickly be imprinted on to any gas cloud(s), so the absorption would likely have a higher velocity dispersion than if it was produced by gas clouds at larger radii in the galaxy, i.e. $\gtrsim 8\,\mathrm{km\,s^{-1}}$. By the same argument, they would have a higher velocity dispersion than absorption lines seen at radii of several hundred pc or more in galaxies where a high redshift quasar has been used as the backlight for absorption (e.g. Wiklind & Combes 1996; Combes 2008; Muller et al. 2013).

4.3 Where is the absorbing gas located in each galaxy?

We have suggested the existence of two types of absorption system. When considering the molecular emission and absorption properties, these two types of absorber are indicated by the line-of-sight velocities, column densities, and velocity dispersions.

In some cases, this seems to concur with claims that these observations are tracing AGN accretion. Where the absorbing gas has inward velocities of several hundreds of $\mathrm{km\,s^{-1}}$, ongoing supermassive black hole accretion has been suggested, e.g. A2597 by Tremblay et al. (2016), S555 and A2390 by Rose et al. (2019b). For a molecular gas cloud at a radius of 100 pc and with an average inward velocity of 500 $\mathrm{km\,s^{-1}}$, the supermassive back hole could be reached in approximately 2×10^5 yr. This is short on galactic time-scales, so if the clouds really are at these distances from the centre of their host galaxy, their accretion is a plausible end result.

We now consider the properties of each absorption system in detail to more tightly constrain the location of the absorbing gas.

(i) **NGC 6868**'s molecular gas is centred on the radio core, extends over approximately 0.5 kpc, and has a mass of $1.3 \pm 0.2 \times 10^8\,\mathrm{M_\odot}$. The gas appears to be in a disc viewed at a small angle of inclination (perhaps 10–20°) and has a velocity range of approximately 300 $\mathrm{km\,s^{-1}}$. We are likely seeing typical clouds in this galaxy (i.e. those away from the core and in the more extended disc) for three reasons. First, the column density of molecular gas along the line

of sight to the continuum is relatively high at 960 $\mathrm{M_\odot\,pc^{-2}}$, so an alignment between the continuum and several of its molecular clouds is expected. This expected column density is also very similar to the actual column density of the absorption (1100 $\mathrm{M_\odot\,pc^{-2}}$). When chance alignments between the continuum and molecular clouds visible in emission are responsible for the absorption, they would likely have velocities which match the emission, as is the case. The absorption regions also have relatively low velocity dispersions ($\sigma = 6.4\,\mathrm{km\,s^{-1}}$, FWHM $= 15\,\mathrm{km\,s^{-1}}$), typical of clouds within the disc of a galaxy.

(ii) **S555**'s molecular gas is poorly resolved and no velocity structure is discernible. However, the gas is heavily concentrated and centred around 200 pc from the radio core, with weak emission extending out to approximately 3 kpc. The total mass is $5.6 \pm 0.2 \times 10^8\,\mathrm{M_\odot}$. In this case, the properties of the absorption indicate that it is not due to the same population of clouds responsible for the emission. The molecular column density is 130 $\mathrm{M_\odot\,pc^{-2}}$ for the gas causing the emission, so the probability of an alignment is small but not insignificant. However, the actual column density of the absorbing gas is 10 times higher than this, and no molecular emission is found at velocities matched to the absorption lines. Indeed, any absorption that does come from the typical gas clouds would be embedded within the emission – at least 200 $\mathrm{km\,s^{-1}}$ below where the absorption is actually present. The gas is therefore moving towards the galaxy centre at high velocity, and a velocity which is significantly different to the gas seen in emission. On the other hand, the velocity dispersion of the absorption is only moderate ($\sigma = 7.2\,\mathrm{km\,s^{-1}}$, FWHM $= 17\,\mathrm{km\,s^{-1}}$). This is lower than might be expected if the clouds were subject to the high velocity gradient close to a supermassive black hole. On the balance of probabilities, the absorbing gas is most likely near the galaxy centre and in the process of accretion. However, due to its moderate velocity dispersion it is unlikely to be in the very centre of the galaxy.

(iii) **Hydra-A** has a 5 kpc wide edge-on molecular gas disc with a total mass of $3.1 \pm 0.2 \times 10^9\,\mathrm{M_\odot}$, a smooth velocity gradient and a velocity range of approximately 700 $\mathrm{km\,s^{-1}}$ (Rose et al. 2019a). Lower angular resolution CO(2–1) observations from IRAM place the mass at $2.26 \pm 0.29 \times 10^9\,\mathrm{M_\odot}$ (Hamer et al. 2014). The molecular gas with velocities matched to the absorption is centred on the radio core (Fig. 1) and extended by a few hundred parsecs along the blueshifted edge of the disc. The column density of molecular gas against the radio core is 530 $\mathrm{M_\odot\,pc^{-2}}$, similar to the 210 $\mathrm{M_\odot\,pc^{-2}}$ derived from the absorption. Estimates of the diameter of the continuum source in Hydra-A have been placed at between 4 and 7 pc, so on average we would expect approximately a few tens of $\sim$170 $\mathrm{M_\odot}$ clouds from the galaxy's disc to lie along the line of sight. Hydra-A is by far the best-studied absorption system of this kind, and this matches the observations of Rose et al. (2020). They identified at least 12 molecular clouds that are responsible for Hydra-A's absorption. The absorbing clouds are also at the peak of the emission profile – the most likely velocity at which we would detect clouds lying in the disc. Additionally, the velocity dispersions of the individual clouds are very low ($<5\,\mathrm{km\,s^{-1}}$, FWHM $<12\,\mathrm{km\,s^{-1}}$). In terms of the number of clouds, their velocities, and velocity dispersions, the absorption in Hydra-A therefore has the properties expected as a result of chance alignments between the continuum and gas clouds in the galaxy's disc.

(iv) **Abell 2390** contains a significant molecular mass of $2.2 \pm 0.6 \times 10^{10}\,\mathrm{M_\odot}$, though due to its relatively high redshift the emission is weak and poorly resolved. Nevertheless, the molecular gas is significantly extended across a strongly asymmetric filamentary

structure approximately 20 kpc long and 5 kpc wide. Evidence of velocity structure to the emission is observed, with higher velocities being found at larger radii (Fig. 3), perhaps indicating a molecular outflow. Abell 2390's molecular emission implies an average column density of molecular gas along the line of sight to the radio core of $160 \, M_\odot \, pc^{-2}$, so the probability of several of the clouds we see in emission aligning with the continuum is small – unless the line of sight passes through a particularly dense clump of the ISM. At 15 000 $M_\odot \, pc^{-2}$, the absorption in Abell 2390 is 92 times stronger than the emission would predict. The absorption also has a dispersion of $52 \, km \, s^{-1}$ (FWHM $= 120 \, km \, s^{-1}$; Rose et al. 2019b) – extremely wide considering it is produced by just 15 000 $M_\odot \, pc^{-2}$ of gas. That implies the absorbing gas is in a region with a very high velocity gradient. Such a gradient can occur within a few parsecs of a supermassive black hole. However, the emission peak from gas on large scales closely matches the absorption line speeds, which may be more than coincidence. The broad, $800 \, km \, s^{-1}$ emission seen towards the nucleus indicates a second emission component that may be associated with the nucleus or an outflow. This complexity prevents a conclusive statement, but due to the high velocity dispersion and inflow speed, the absorbing gas is probably close to the core and accreting on to the AGN.

(v) **Abell 1644** has $1.6 \pm 0.3 \times 10^9 \, M_\odot$ of molecular gas, the bulk of which is contained in four main clumps distributed along an arc extending out from the galaxy centre. This arc of gas has been spatially matched to X-ray emission, suggesting it has cooled from the hot intracluster medium (Baek et al. 2022). Two of the gas clumps are within approximately 200 pc of the radio core, while the others are at radii of approximately 7 and 10 kpc. The absorption in Abell 1644 is close to the peak of the spatially matched emission. This implies that the absorption is due to a sample of the same clouds responsible for the emission. The velocity dispersion is relatively high, ($\sigma = 11 \, km \, s^{-1}$, FWHM $= 26 \, km \, s^{-1}$), though from more recent ALMA observations of HCO$^+$, we know this is due to it containing multiple components (Rose et al., in preparation). The column density of molecular gas along the line of sight to the radio core has a lower limit of $>50 \, M_\odot \, pc^{-2}$, so we are unable to say how much gas from the emitting population would be expected to lie along the line of sight (this is a lower limit because the molecular emission coincident with the radio core is unresolved in a relatively large beam). Nevertheless, even the upper limit this gives for the clumping factor (<6) implies that the absorption is not tracing significantly more gas than the emission would predict. This, combined with the line-of-sight velocity and velocity dispersion of the absorption implies that the absorption in Abell 1644 is caused by typical clouds within the galaxy.

(vi) **IC 4296** has a molecular mass of $2.3 \pm 0.2 \times 10^7 \, M_\odot$ in a disc-like structure approximately 0.8 kpc wide and with a weak velocity gradient (Ruffa et al. 2019, find a molecular mass of $2.0 \pm 0.2 \times 10^7 \, M_\odot$). The angular resolution of the observation is poor, so only an upper limit of 0.2 kpc can be placed on the disc's width. Emission with velocities matched to the absorption is spread across most of the disc-like structure, except at its extremities. The properties of the molecular absorption are entirely consistent with it being due to clouds within the disc of the galaxy. The covering factor of the continuum is $170 \, M_\odot \, pc^{-2}$, similar to the actual column density of the absorption along the line of sight of $290 \, M_\odot \, pc^{-2}$. The absorption also has a narrow velocity dispersion (for the deepest line, $\sigma = 4 \, km \, s^{-1}$, FWHM $= 9.4 \, km \, s^{-1}$) and the absorbing clouds lie at the peak of the molecular emission.

(vii) **Abell 2597** has an approximately 10 kpc wide concentration of molecular gas centred on its radio core, with a velocity range of

$200 \, km \, s^{-1}$. More diffuse emission extends 30 kpc out to the north and south, taking the total molecular mass to $4.6 \pm 0.5 \times 10^9 \, M_\odot$ (Tremblay et al. 2018, find a mass of $3.2 \pm 0.1 \times 10^9 \, M_\odot$. From the extraction region they show, this mass likely includes less of the extended emission). In Figs 2 and 3, we only show the nuclear region, but wider maps can be seen in Tremblay et al. (2018). Molecular emission with velocities matched to the absorption lies outside the radio core, at radii between 300 pc and 3 kpc. The column density of molecular gas towards the continuum is estimated at $130 \, M_\odot \, pc^{-2}$, so on average only a small number of clouds would be expected to cover the continuum. This is in stark contrast to the absorption's actual column density of $6800 \, M_\odot \, pc^{-2}$, suggesting it is not caused by the same population of clouds responsible for the emission. The line-of-sight velocities of the absorbing gas clouds are also dissimilar to those causing the molecular emission. Furthermore, the width of the three resolved absorption features is moderately high (roughly $\sigma = 9 \, km \, s^{-1}$, FWHM $= 21 \, km \, s^{-1}$ for each component). This is higher than is typically seen for absorption due to molecular clouds at several hundreds of parsec or more from their galaxy centre (e.g. Wiklind & Combes 1996; Muller et al. 2013). All the properties of the absorption in this system suggest the gas is most likely in the central regions of the galaxy. Due to the high velocity towards the core, accretion can be inferred.

(viii) In **NGC5044**, the highest spatial resolution observations of the molecular gas are with CO(1–0), and suggest a mass of $2.4 \pm 0.4 \times 10^7 \, M_\odot$ [with CO(2–1) Schellenberger et al. 2020, find a mass of $4.2 \pm 0.1 \times 10^7 \, M_\odot$]. The weak CO(1–0) emission is offset from the continuum by around 300 pc. An accurate estimate of its diameter is hard to attain due to the weakness of the emission, but it may be up to 1.5 kpc. No emission is detectable along the line of sight to the radio core, so only a $<50 \, M_\odot \, pc^{-2}$ upper limit for the column density of emitting gas can be found, much lower than the actual $3800 \, M_\odot \, pc^{-2}$ column density of the absorbing gas. This, combined with the absorption being at least $100 \, km \, s^{-1}$ offset from the emission implies that the absorbing clouds are not drawn from the population visible in emission. Instead, they are more likely close to the galaxy centre where their probability of intersecting the continuum is relatively high. However, although the absorbing gas is moving inwards at $280 \, km \, s^{-1}$ and is likely close to the galaxy centre, we cannot definitively confine it to the immediate surroundings of the radio core because its velocity dispersion ($\sigma = 5.9 \, km \, s^{-1}$, FWHM $= 14 \, km \, s^{-1}$) is lower than might be expected in this region.

4.4 Constraining the location of typical absorbing clouds

Since the absorbing gas in Figs 1 and 2 is observed against the host galaxy's bright radio core, we can be certain of its location in terms of its RA and Dec. In four galaxies in our sample – S555, Abell 2390, Abell 2597, and NGC 5044 – we find the absorbing gas is likely in the galaxy centre.

In the other four galaxies, the absorption is most likely caused by typical clouds within the galaxy. These could be at any radius at which molecular emission is present, but we now attempt to constrain the location of the absorbing gas by isolating the emission which has velocities equal to the absorbing gas.

In Fig. 6, we show the flux contained within increasing radii from the core as a fraction of the total flux. This is done using the two flux density maps for each of the sources shown in Figs 1 and 2, i.e. using one map made with the emission present at all velocities, and one made with the emission present at velocities matched to the absorption. In Table 5, we show half-light radii derived from Fig. 6, and the maps shown in Figs 1 and 2. These values serve as estimates
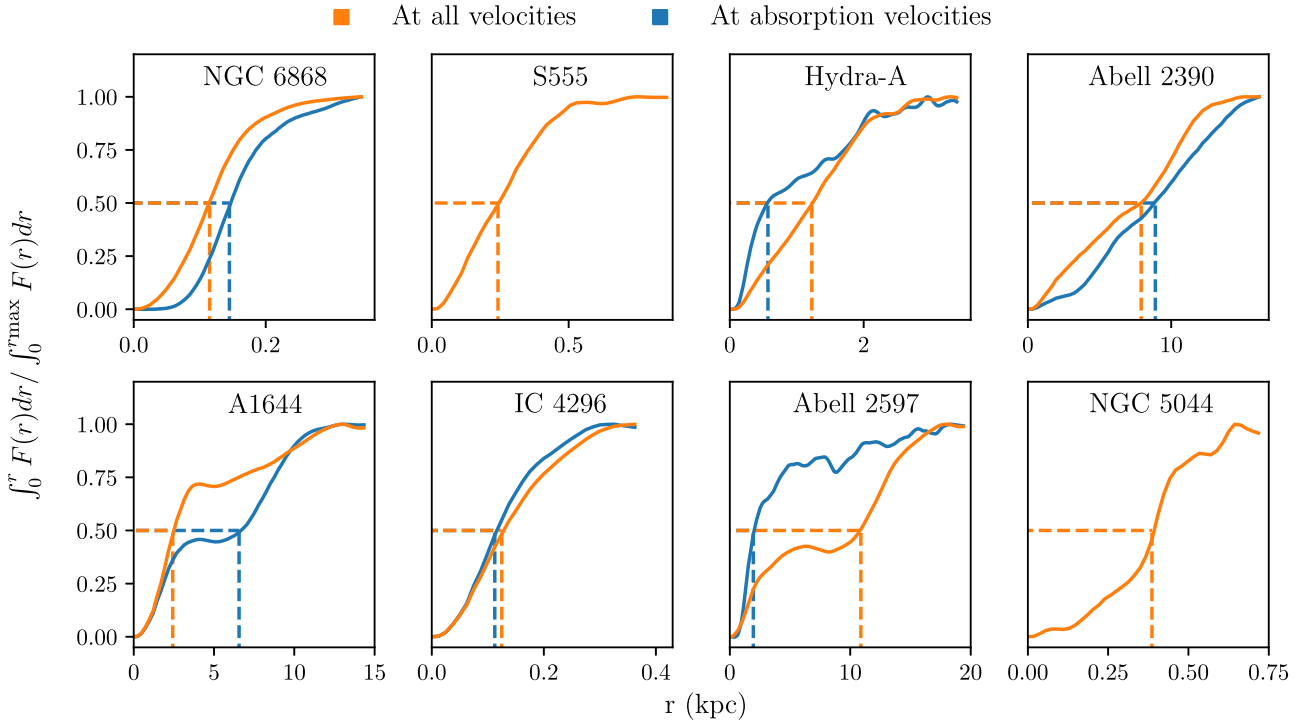
Figure 6. The fraction of the CO flux contained within a given radius, for flux at all velocities (orange) and velocities which match that of the absorption regions (blue). Blue and orange dashed lines indicate the half-light radii. This effectively gives an upper limit for the probability that a randomly selected gas cloud will lie within a given radius. This acts as an upper limit because the observations only show the tangential distance from the radio core, and not the line-of-sight distance. It is reasonable to assume the flux-to-mass ratio is constant within each galaxy, so this also serves to illustrate the fraction of the molecular mass which is contained within a given radius.

Table 5. Half-light radii in kpc for CO emission seen at (i) all velocities and (ii) velocities matched to the absorption lines seen against each galaxy's radio core. These values are found using the maps shown in Figs 1 and 2. See also Fig. 6.

	All velocities	Absorption velocities
NGC 6868	0.11	0.15
S555	0.24	0.64
Hydra-A	1.2	0.56
Abell 2390	7.9	8.9
Abell 1644	2.4	6.6
IC 4296	0.13	0.11
Abell 2597	11	2.0
NGC 5044	0.39	0.26

of the median radius at which a typical molecular gas cloud will be, and a gas cloud with the same velocity as the absorbing gas. Inferences from this must be treated with caution because the curves in Fig. 6 are found using molecular emission seen in a tangential plane to the one in which the absorbing gas lies. Assuming the gas within these galaxies is approximately spherically symmetric, the half-light radii serve as reasonable estimates for the most likely location of the absorbing gas clouds.

4.5 The infall velocities of molecular clouds

We have proposed that four systems in Figs 1 and 2 are likely to contain absorption due to molecular gas clouds close to the centre of the host galaxy. Due to their high inward velocities, in time these clouds are likely to be accreted by the AGN.

However, as the moments maps show, these clouds have velocities which are similar to many others visible in emission up to several kpc out from the galaxy centre. This similarity in the velocities of two cloud populations in very different environments may be considered surprising, and some mechanism may be acting to prevent the clouds accreted by an AGN from having strongly dissimilar velocities to those which are considerably further out. Simulations suggest that this is the case, with inward radial motions significantly higher than the projected velocities of our absorption lines (i.e. intrinsic velocities of above 1000 $km\,s^{-1}$) rarely occurring at radii above 1 pc. When they do occur, these velocities are held only by the few clouds that have experienced major inelastic collisions (Gaspari et al. 2013).

The clouds we infer to be accreting are detected against the galaxy's central continuum source, and have inward line-of-sight velocities of hundreds of $km\,s^{-1}$. However, they will also have tangential velocity components and will therefore not be in free-fall. Instead, they will be on more stable elliptical orbits that can decrease over time due to losses of energy and momentum (e.g. by cloud–cloud collisions; Gaspari et al. 2013). Due to the proximity to the galaxy centre, the outward force of ram-pressure stripping can also act to dampen any increases in velocity towards the galaxy centre caused by the strong gravitational field (Combes 2018). This places an upper limit on the infall velocity attainable by molecular clouds, and may have detectable effects when their absorption features are seen with different tracers, such as other molecular lines or H I.

4.6 Perturbed CO emission and AGN accretion

From our sample of eight galaxies with both molecular emission and absorption, four have absorption which is likely due to clouds

accreting on to their AGN (S555, Abell 2390, Abell 2597, NGC 5044). The other four have absorption which is likely due to typical clouds at much larger radii (NGC6868, Hydra-A, Abell 1644, and IC 4296). Interestingly, those with absorption likely due to clouds accreting on to the AGN have irregular velocity structures (Fig. 3), while those with absorption due to typical clouds have smooth molecular emission profiles.

An irregular and disturbed velocity structure in a galaxy's molecular emission may therefore be conducive to fuelling of the AGN. This would likely be due to increased cloud–cloud collisions, which cause a loss of angular momentum and lead to clouds falling to lower orbits.

In the three galaxies in our sample which contain emission but no absorption (Fig. 4), one has a smooth velocity structure (RXC J1350.3+0940), while two are irregular (MACS 1931.8−2634 and RXC J1603.6+1553). Although there is no detectable absorption in these systems, we have provided upper limits in Table 4. By comparing these upper limits with the absorption column densities in the other galaxies, we can judge whether or not their lack of absorption is due to the sensitivity of the observations.

Where we find absorption due to typical clouds, the column densities (1100, 210, 310, 290 $M_\odot\,pc^{-2}$) are lower than in cases where the absorption is due to clouds undergoing AGN accretion (1300, 15 000, 6800, 3800 $M_\odot\,pc^{-2}$). For the systems in which there is molecular emission only, the absorption upper limits are (<700, 2200, and $<3400\,M_\odot\,pc^{-2}$). Assuming the dichotomy in the absorption column densities of the two types of absorber is more than coincidence, these upper limits mean we cannot rule out the presence of undetected absorption due to typical clouds. However, there is a much lower probability that they contain absorption due to clouds accreting on to their AGN. Two of these three systems contain a disturbed velocity structure, so deep and wide absorption due to accreting clouds is unlikely to be a universal feature of galaxies with irregular velocity structures.

4.7 Limitations to our classifications

So far we have restricted our classification of these absorption systems, suggesting they are likely due to alignments between the continuum and (i) a small fraction of the clouds we see in emission, or (ii) clouds near the galaxy centre that are in the process of accreting on to the AGN. However, there is no reason to believe a dichotomy exists i.e. that no systems combine these two types of absorption. The X-ray selected Rose et al. (2019b) survey in which most of the absorption systems we present were identified had a detection rate of around 40 per cent. Given that we find a roughly equal prevalence of the two types of absorber, the detection rate of each can be approximated to 20 per cent. If they can be treated as independent, absorption of both types will be detectable in around four per cent of sources (though this could rise with more sensitive observations).

In Fig. 5, we noted differences between the clumping factors of the two types of absorber. Systems with absorption due to accreting clouds have much higher clumping factors than those due to the galaxy's molecular clouds that are visible in emission (Fig. 5). If a system's absorption is due to typical clouds within the galaxy, high clumping factors may also be caused by significant inhomogeneities in the ISM. Therefore, we do not yet have reason to believe that high clumping factors are an integral or unique property of systems that have molecular absorption due to clouds accreting on to their AGN. With greater sensitivity, we may find absorption with high velocity dispersions and high velocities towards the galaxy centre, but which are relatively weak.

5 CONCLUSIONS

We have analysed ALMA observations of eight galaxies with both molecular emission and absorption and constrained the location of their absorbing gas. We also show observations of three massive galaxies with only molecular emission lines. Our findings can be summarized as follows:

(i) We introduce the 'clumping factor' of molecular absorption line systems – the ratio of two column densities along the line of sight to a galaxy's continuum source. The first is estimated from the molecular emission spatially coincident with the radio core. This gives the amount of gas from across the galaxy that covers a typical line of sight to the continuum source. The second is the actual column density of molecular gas covering the continuum, estimated from the absorption lines.

(ii) When comparing the clumping factors and the FWHM of the absorption lines in our sample with the velocities of their molecular absorption lines (Fig. 5), two distinct populations become apparent. One has low clumping factors, lower FWHM and molecular absorption at close to $0\,km\,s^{-1}$. The others have high clumping factors of $\gtrsim 10$, higher FWHM and the absorbing gas has high inward velocities towards the galaxy centre.

(iii) We argue that those with low clumping factors, lower FWHM, and absorption close to $0\,km\,s^{-1}$ are due to chance alignments between the continuum source and a fraction of the same molecular clouds responsible for the galaxy's molecular emission. The low velocity dispersions in these systems are similar to those found for absorption far out from galaxy centres using background quasars. Additionally, since the absorption is due to chance alignments between the continuum source and a fraction of the molecular clouds that are visible in emission, the absorption is always embedded within that emission.

(iv) Absorbers with high clumping factors, higher FWHM and high inward velocities are likely created by gas clouds accreting on to their host AGN. The absorption in these systems is unlikely to have been produced in the same manner as described above for two main reasons. First, the clumping factors consistently imply that at least an order of magnitude more absorption is being detected than is predicted from the emission. Secondly, the absorption lines are significantly redshifted compared with the molecular emission (except in Abell 2390, which has $900\,km\,s^{-1}$ wide emission). If the absorption was produced by the same population of clouds responsible for the emission, absorption would be most likely to occur at or near the peak of that emission.

(v) Clouds accreting on to their AGN are much less numerous than those throughout a galaxy that make up the molecular emission profile. Their scarcity means they are not visible in emission, while their proximity to the galaxy centre means they are relatively more likely to align with the continuum source.

(vi) We present the first molecular mass estimates for five brightest cluster galaxies. Three of these have molecular absorption lines against their central continuum source (NGC6868, S555, A2390) and two do not (RXC J1350.3+0940, RXC J1603.6+1553).

(vii) Three of the brightest cluster galaxies we present have molecular masses of $>10^{10}\,M_\odot$, but lack molecular absorption lines. This is surprising given their masses are two or more orders of magnitude higher than in several other absorbing sources. The column density of molecular gas covering the continuum source is a better predictor of absorption due to alignments between the continuum and a fraction of the clouds visible in emission.

DATA AVAILABILITY

The vast majority of the data underlying this article are publicly available from the ALMA archive. The CO(2–1) observation of NGC6868 will become publicly available on 2022 November 25. Before then, it will be shared on reasonable request to the corresponding author.

REFERENCES

Abazajian K. N. et al., 2009, ApJS, 182, 543
Baek J., Chung A., Edge A., Rose T., Kim J.-W., Jung T., 2022, ApJ, 932, 64
Boizelle B. D., Barth A. J., Darling J., Baker A. J., Buote D. A., Ho L. C., Walsh J. L., 2017, ApJ, 845, 170
Bolatto A. D., Wolfire M., Leroy A. K., 2013, ARA&A, 51, 207
Braine J., Combes F., 1992, A&A, 264, 433
Combes F., 2008, Astrophys. Space Sci., 313, 321
Combes F., 2018, preprint (arXiv:1807.07027)
Crawford C. S., Allen S. W., Ebeling H., Edge A. C., Fabian A. C., 1999, MNRAS, 306, 857
David L. P. et al., 2014, ApJ, 792, 94
Donahue M., de Messières G. E., O'Connell R. W., Voit G. M., Hoffer A., McNamara B. R., Nulsen P. E. J., 2011, ApJ, 732, 40
Edge A. C., Wilman R. J., Johnstone R. M., Crawford C. S., Fabian A. C., Allen S. W., 2002, MNRAS, 337, 49
Fabian A. C., Ferland G. J., Sanders J. S., McNamara B. R., Pinto C., Walker S. A., 2022, MNRAS, 515, 3336

Fogarty K. et al., 2019, ApJ, 879, 103
Gaspari M., Ruszkowski M., Oh S. P., 2013, MNRAS, 432, 3401
Gaspari M., Temi P., Brighenti F., 2017, MNRAS, 466, 677
Gaspari M., Tombesi F., Cappi M., 2020, Nat. Astron., 4, 10
Godard B., Falgarone E., Gerin M., Hily-Blant P., de Luca M., 2010, A&A, 520, A20
Hamer S. L. et al., 2014, MNRAS, 437, 862
Hamer S. L. et al., 2016, MNRAS, 460, 1758
Harris C. R. et al., 2020, Nature, 585, 357
Hughes A. et al., 2010, MNRAS, 406, 2065
Hunter J. D., 2007, Comput. Sci. Eng., 9, 90
Jaffe W., Bremer M. N., Baker K., 2005, MNRAS, 360, 748
Jones E., Oliphant T., Peterson P., 2011, SciPy Open Source Scientific Tools for Python, www.scipy.org
Krumholz M. R., Kruijssen J. M. D., Crocker R. M., 2016, MNRAS, 466, 1213
Lombardi M., Alves J., Lada C. J., 2010, A&A, 519, L7
McMullin J. P., Waters B., Schiebel D., Young W., Golap K., 2007, in Shaw R. A., Hill F., Bell D. J., eds, ASP Conf. Ser. Vol. 376, Astronomical Data Analysis Software and Systems XVI. Astron. Soc. Pac., San Francisco, p. 127
McNamara B. R., Russell H. R., Nulsen P. E. J., Hogan M. T., Fabian A. C., Pulido F., Edge A. C., 2016, ApJ, 830, 79
Mangum J. G., Shirley Y. L., 2015, PASP, 127, 266
Miville-Deschênes M.-A., Murray N., Lee E. J., 2017, ApJ, 834, 57
Morganti R., 2017, Frontiers Astron. Space Sci., 4, 42
Muller S., Guelin M., 2008, A&A, 491, 739
Muller S. et al., 2013, A&A, 551, A109
Nulsen P. E. J., McNamara B. R., Wise M. W., David L. P., 2005, ApJ, 628, 629
Olivares V. et al., 2019, A&A, 631, A22
Pineda J. L., Velusamy T., Langer W. D., Goldsmith P. F., Li D., Yorke H. W., 2010, A&A, 521, L19
Pizzolato F., Soker N., 2005, ApJ, 632, 821
Pulido F. A. et al., 2018, ApJ, 853, 177
Rachford B. L. et al., 2009, ApJS, 180, 125
Robitaille T., Bressert E., 2012, Astrophysics Source Code Library, record ascl:1208.017
Rose T. et al., 2019a, MNRAS, 485, 229
Rose T. et al., 2019b, MNRAS, 489, 349
Rose T. et al., 2020, MNRAS, 496, 364
Ruffa I. et al., 2019, MNRAS, 484, 4239
Schellenberger G. et al., 2020, ApJ, 894, 72
Solomon P. M., Rivolo A. R., Barrett J., Yahil A., 1987, ApJ, 319, 730
Temi P., Amblard A., Gitti M., Brighenti F., Gaspari M., Mathews W. G., David L., 2018, ApJ, 858, 17
The Astropy Collaboration, 2013, A&A, 558, A33
The Astropy Collaboration, 2018, AJ, 156, 123
Tremblay G. R. et al., 2016, Nature, 534, 218
Tremblay G. R. et al., 2018, ApJ, 865, 13
van der Walt S., Colbert S. C., Varoquaux G., 2011, Comput. Sci. Eng., 13, 22
Van Rossum G., Drake F. L., 2009, Python 3 Reference Manual. CreateSpace, Scotts Valley, CA
Virtanen P. et al., 2020, Nat. Methods, 17, 261
Voit G. M., Donahue M., 1997, ApJ, 486, 242
Wiklind T., Combes F., 1996, Nature, 379, 139

This paper has been typeset from a TEX/LATEX file prepared by the author.